Oceanologia, corrected, in press
Polish Academy of Sciences
Institute of Oceanology

https://doi.org/10.5697/JZIS4816

The influence of seasonal hydrography and nutrient regimes on micro-phytoplankton assemblages in the coastal waters of Jeddah, central Red Sea

Reny Palliparambil Devassy[1], Vidyanandan Remadevi Shamji[2], Faisal Mana Alsaaq[2], Turki Metabe Alraddadi[3], Mohsen Mohamed El-Sherbiny[4,*]

Abstract
This study examined spatial and temporal variations in hydrography, nutrients, and phytoplankton along the Jeddah coast, Red Sea. Temperature ranged from 26.2 ± 0.14°C (February) to 33.4 ± 0.17°C (August), with minimal salinity changes. Nitrate, silicate, and SPM were elevated in the central region. Chlorophyll *a* and phytoplankton abundances peaked there, reaching 1.54 mg m^{-3} in October and $43{,}393 \times 10^3$ cells m^{-3} in July. Centric diatoms (*Proboscia alata*) dominated in summer, pennate diatoms (*Lioloma elongatum*) in May, and dinoflagellates in June (1246×10^3 cells m^{-3}). Cyanophytes peaked in November. In total, 284 species, including 40 harmful taxa, were identified, mainly diatoms and dinoflagellates.

Keywords
Phytoplankton; Anthropogenic influences; Abundance; Coastal waters; Red Sea

[1]*Almobdioon Center for Studies, Consultancy, and Training, King Abdulaziz University, Jeddah, Saudi Arabia*
[2]*Faculty of Maritime Studies, King Abdulaziz University, P.O Box 80401, Jeddah, Saudi Arabia*
[3]*Department of Marine Physics, Faculty of Marine Science, King Abdulaziz University, P.O Box 80207, Jeddah 21589, Saudi Arabia*
[4]*Department of Marine Biology, Faculty of Marine Science, King Abdulaziz University, P.O Box 80207, Jeddah 21589, Saudi Arabia*
***Correspondence**: ooomar@kau.edu.sa (M.M. El-Sherbiny)

Received: 14 October 2025; **revised:** 30 November 2025; **accepted**: 22 December 2025

1. Introduction

Phytoplankton constitute the primary foundation of marine food webs and play a vital role in maintaining the health and functioning of ocean ecosystems (Reynolds, 2008; Naselli-Flores and Padisák, 2023). Beyond supporting aquatic productivity, these microscopic organisms play a crucial role in global biogeochemical processes, particularly in carbon cycling and oxygen production (Falkowski, 1994; Schoo et al., 2013; Robinson, 2017). Through photosynthesis, phytoplankton fix atmospheric carbon dioxide; a fraction of this carbon is transferred through the marine food web or transported to deeper ocean layers through the biological carbon pump, which transfers organic carbon to depth (Richardson and Jackson, 2007; Durkin et al., 2016; Richardson, 2019). This mechanism is critical in sequestering carbon for long periods, thus mitigating the impacts of climate change by regulating atmospheric CO_2 concentrations. Additionally, phytoplankton are primary contributors to the global oxygen balance, producing nearly half of the Earth's oxygen supply (Falkowski, 1994). However, because of their sensitivity to environmental changes, any alteration in surrounding physical, chemical, or biological parameters can disrupt their dynamics, causing chain reactions that impact various components of the marine ecosystem (Häder and Gao, 2015; Salmaso and Tolotti, 2021). Consequently, monitoring phytoplankton variability is essential for understanding ocean productivity, ecosystem stability, and the broader implications of global climate change (Henson et al., 2021).

As primary producers surviving in an extremely oligotrophic environment, phytoplankton in the Red Sea ecosystem face significant challenges to their growth and proliferation (Rasul et al., 2018). The naturally low nutrient concentrations in these waters limit primary productivity, making phytoplankton survival highly dependent on sporadic external inputs. Compounding these constraints, the region's hot and arid climate further exacerbates environmental stress, creating conditions that are often unfavorable for phytoplankton growth and sustainability (Raitsos et al., 2011). The scarcity of rainfall and the near absence of riverine discharge along the eastern coast of the Red

Sea result in minimal terrestrial nutrient input (Morcos, 1970). Instead, the region relies heavily on alternative nutrient sources, mainly through the inflow of nutrient-rich waters from the Indian Ocean via the Bab-el-Mandeb Strait and periodic winter upwelling events, which temporarily replenish surface nutrients (Sofianos and Johns, 2003; Wafar et al., 2016). Although much of the Red Sea ecosystem remains characteristically oligotrophic, notable changes have been observed in several of its coastal regions (Devassy et al., 2017; Carvalho et al., 2019). Increasing anthropogenic influences, particularly near rapidly expanding urban centers and densely populated coastal areas have begun to alter the natural oligotrophic status of these waters (Ghandour et al., 2014; Cai et al., 2024). Inputs from domestic, industrial, and recreational activities are contributing to localized nutrient enrichment, which, in turn, is impacting the ecological balance of these regions (Peña-García, 2022). These shifts are increasingly reflected in the composition and dominance patterns of phytoplankton communities, indicating a departure from the typical low-nutrient, low-biomass conditions that define much of the Red Sea.

Jeddah, a rapidly expanding metropolitan city along the eastern coast of the Red Sea, serves as a prominent example of growing anthropogenic pressures on coastal marine ecosystems (Peña-García et al., 2014). In recent years, the region has experienced several eutrophication events, signaling a departure from the traditionally oligotrophic conditions of the Red Sea (Al-Amri et al., 2020; El-Sherbiny et al., 2021). Localized nutrient enrichment – driven by urban runoff, sewage discharge, and coastal development – poses significant threats to marine biodiversity, particularly to the region's historically pristine coral reef ecosystems (Turki and Mudarris, 2008). A growing concern is the increasing occurrence of phytoplankton species capable of forming harmful algal blooms (HABs) in coastal waters (Mohamed, 2018). The Jeddah coastline, in particular, is witnessing an increasing frequency of such events, raising serious ecological and management challenges for the sustainability of marine resources and ecosystem health in the area (Gomaa et al., 2018; Al-Aidaroos et al., 2019). Continuous monitoring of phytoplankton abundance and diversity is therefore essential for assessing the ecological health of coastal waters and mitigating the impacts of eutrophication and HAB events (Al-Yamani et al., 2024; Ismael and Alkawri, 2024). Regular observation not only enables the early detection of shifts in community structure but also supports the identification of emerging HAB-forming species (Cullen, 2008). Establishing a comprehensive and region-specific phytoplankton database would serve as a valuable tool for both ecological research and management. Such a database would facilitate the long-term study of species diversity, track temporal and spatial trends, and aid in distinguishing potentially harmful taxa from benign ones.

The present study investigated monthly phytoplankton diversity across three distinct zones along the Jeddah coastal region of the central Red Sea, each representing varying degrees of anthropogenic influence. The northern zone, characterized by minimal human impact, serves as a relatively pristine reference site. In contrast, the central zone is subjected to inputs from sewage discharge and desalination plant effluents, while the southern zone is influenced by the operations of a major international port and the presence of sewage accumulation and treatment facilities. This spatial approach enables comparison of phytoplankton community composition under varying environmental pressures. Furthermore, the study extends beyond the immediate coastline to include adjacent offshore stations, thereby capturing the extent to which coastal anthropogenic activities influence broader marine ecosystems.

2. Material and methods

2.1 Study sites

A total of 12 study sites were chosen in the coastal region of Jeddah, a rapidly developing metropolitan city located in the Red Sea basin. The selected sites were representative of the northern, central, and southern regions of the area. Four sites were chosen from the northern region (1A–2B), which is generally considered to be a pristine environment. Four sites were chosen from both the central (3A–4B) and southern regions (5A–6B), where anthropogenic influences are more pronounced (Figure 1). In the central zone's coastal area, there is a desalination plant and a sewage disposal site. The southern zone contains the Jeddah International port, a sewage disposal site, and two natural lagoons that suffer from severe man-made pollution. Six of the selected sites were located in close proximity to the coast (1A–6A), while the remaining six (1B–6B) were located 4 km away from the coastal sites (Figure 1).

2.2 Sampling strategy

All stations were sampled on a monthly basis for a year in 2019–2020 (January–December). Sea surface temperature and salinity were measured using a portable water quality measuring probe (Horiba U50), while water samples were collected from a depth of 50 cm using a 5-L Niskin sampler (Hydrobios). For chlorophyll *a*, 4–6 L of seawater was collected in clean, acid-washed plastic carboys. For nutrients, samples were collected separately in 500 ml Nalgene bottles, and all water samples were kept in the shade until reaching the shore laboratory. Phytoplankton samples were collected using a 20-μm plankton net (Hydrobios) towed horizontally for 5 minutes at a boat speed of 1 knot. The mouth area of the plankton net, with a diameter of 40 cm, was calculated using the formula πr^2. Flow meter readings were recorded immediately before and after each tow, and the distance traveled by the net was determined

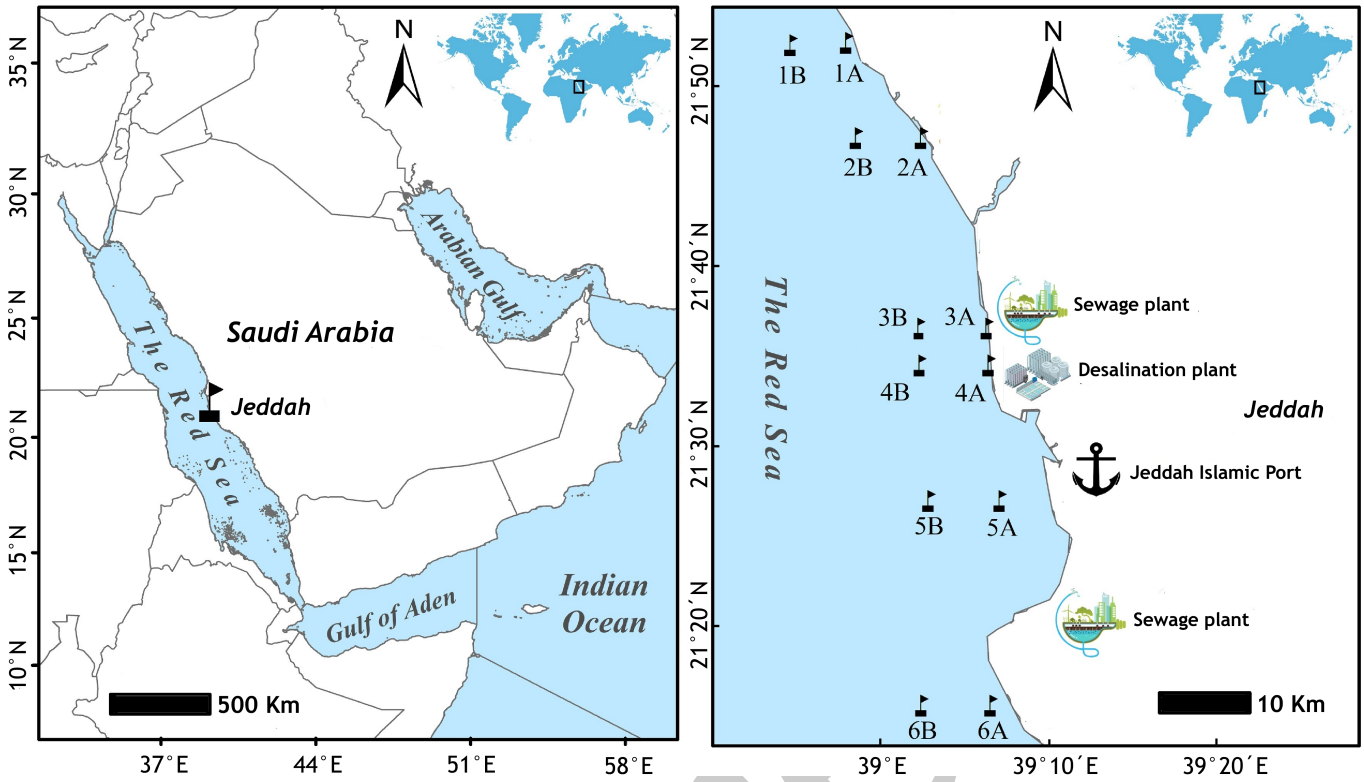

Figure 1. Map showing the sampling stations along the coastal waters of Jeddah, Saudi Arabia.

from the difference between the final and initial readings, multiplied by the calibration factor (0.3 m per revolution). The volume of water filtered (V) in cubic meters was then estimated as follows:

$$V = \pi r^2 \times D$$
$$D = (F_{\text{final}} - F_{\text{initial}}) \times 0.3 \quad (1)$$

The current study had an annual mean vwf of 5.19 ± 4.99 m^3. The samples were later promptly fixed in amber glass bottles using Lugol's iodine solution along with a few drops of concentrated formaldehyde (Kürten et al., 2015). Upon reaching the laboratory, seawater samples were filtered through Whatman GF/F filters (0.7 μm) and Whatman Nucleopore membrane filters (0.2 μm) for chlorophyll *a* and nutrient estimation, respectively. Filter papers and water for nutrients were stored at −20°C for further analysis. Chlorophyll *a* concentrations and nutrient levels were determined using a Shimadzu UV spectrophotometer, following the standard procedures described by Parsons et al. (1984). Chlorophyll *a* was extracted from GF/F filters using 90% acetone. The filters were kept overnight at 4°C in the dark to ensure complete pigment extraction. Acidification was performed using 1 N HCl to correct for phaeopigment interference, and absorbance readings were taken at 665 and 750 nm before and after acidification. Chlorophyll *a* concentrations were calculated using the spectrophotometric equations of Parsons et al. (1984):

$$\text{Chl-}a\ (\text{mg m}^{-3}) = \frac{26.7\,[(A_{665} - A_{750})_{\text{before}} - (A_{665} - A_{750})_{\text{after}}]\,V_{\text{extract}}}{V_{\text{filtered}} L} \quad (2)$$

where V_{extract} is the extract volume (mL), V_{filtered} is the volume of water filtered (L), and L is the cuvette path length (cm). This procedure ensured accurate quantification of chlorophyll *a*, with appropriate correction for phaeopigments and consistent QA/QC practices. Nutrient concentrations were measured following the colorimetric protocols of Parsons et al. (1984) using 0.2 μm filtered seawater. All filtrates were analyzed within 24 hours of collection. Instrument calibration was carried out using freshly prepared multipoint standards, with reagent blanks and duplicate samples included for QA/QC. Analytical precision and detection limits followed the specifications outlined in Parsons et al. (1984). The suspended particulate matter (SPM) was estimated by filtering 1 L of seawater through a pre-weighed Millipore membrane filter (0.45 μm pore size). The filters were then dried at 60°C to constant weight, and SPM concentration was calculated from the difference between pre- and post-drying filter weights and expressed in mg L^{-1}. This temperature was selected to avoid loss of volatile material, and duplicate measurements were performed to ensure analytical precision. The phytoplankton samples were pre-screened using a 500-μm

mesh prior to identification to avoid large-sized zooplankton particles trapped in the samples during the sampling process. The process of phytoplankton enumeration was conducted using a Sedgwick rafter counting chamber, following the standard protocols of LeGresley and McDermott (2010). After the sample was thoroughly homogenized, a 1-mL aliquot was carefully introduced into the counting chamber using a micropipette. The loaded chamber was allowed to settle for a predetermined period to ensure uniform particle distribution prior to microscopic examination. Subsequently, four transects were randomly selected for observation, each comprising 200 microscopic grid units (50 mm × 20 mm × 1 mm). These transects were systematically analyzed to document and enumerate the phytoplankton taxa present. To ensure analytical precision, each sample was counted three times (triplicate analyses), and the resulting data were used to compute total phytoplankton abundance (cells m^{-3}) following established standard calculation protocols. Species identification was performed with the help of phytoplankton monographs like Taylor (1976) and Tomas (1997), and the identified species were cross-checked with WoRMS (World Register of Marine Species) http://www.marinespecies.org/ and http://www.algaebase.org/, following the latest nomenclature. Harmful algal species detected in this study were classified according to the UNESCO (IOC) taxonomic reference list of harmful microalgae (https://www.marinespecies.org/hab).

2.3 Statistical analyses

Pearson's correlation coefficient (r) was used to assess the relationships between various physicochemical and biological parameters. To evaluate the spatial and temporal variations of both biotic and abiotic variables during the study period, one-way ANOVA was performed. Both analyses were conducted using SPSS (version 23). To investigate differences in abiotic variables between stations with higher phytoplankton abundance (stations 3 and 4) and the remaining stations, independent t-tests were applied, using two-tailed p-values and 95% confidence intervals. Prior to performing the t-tests, the D'Agostino and Pearson omnibus normality test was used to determine whether parametric or nonparametric tests (Mann-Whitney U-test) were appropriate. These analyses were performed using GraphPad Prism. To assess spatial variation in phytoplankton community structure, β-diversity analysis was conducted using the one-way ANOSIM method (Anderson et al., 2011). This analysis was carried out monthly to evaluate temporal differences in community composition across the six transects. The analysis was based on the Bray-Curtis similarity matrices of the fourth root transformed abundance of species of phytoplankton of each sampling location. Phytoplankton communities of all six locations were used for the study. The BIO-ENV procedure was employed to identify the combination of environmental variables that best explained the abundance and distribution of the phytoplankton community. For the analysis, fourth-root-transformed data was used for both biotic and abiotic variables. Bray-Curtis similarity matrix was used for the biotic variables, whereas Euclidean distance similarity matrix was used for the abiotic variables and none of the variables were normalized. In addition, redundancy analysis (RDA) was performed using chlorophyll *a* and the abundances of different phytoplankton groups as response variables, whereas environmental variables were used as explanatory factors (temperature, salinity, SPM, and nutrients). The $\log_e$-transformed data were used for the analysis. Biodiversity indices were also calculated to gain a deeper insight into phytoplankton distribution patterns and community structure. All multivariate and ecological analyses, including ANOSIM, BIO-ENV, and RDA, were carried out using PRIMER 7 software.

3. Results

3.1 Temperature salinity

Temperature measurements taken during the study did not display any significant spatial variation, as all readings were taken within a 2-hour timeframe. However, there was noticeable variation over time, with August (33.4 ± 0.17°C) being the warmest month and February (26.2 ± 0.14°C) being the coldest (Figure 2a). In contrast, the study found minimal temporal variation in salinity, with the highest readings (39.4 ± 0.024) observed in August and the lowest readings (38.7 ± 0.041) in February (Figure 2b).

3.2 Inorganic nutrients and suspended particulate matter

Except for the central zone, the nitrate (NO_3^-) values were generally lower throughout the study period. The central zone exhibited higher values, with the highest annual average being reported at station 4A (0.44 ± 0.22 μmol L^{-1}). In contrast, the northern zone had lower nitrate values, with the lowest annual average recorded at station 2B (0.12 ± 0.22 μmol L^{-1}), compared to the other two zones (Figure 3a). The nitrite values (NO_2^-) did not show any significant difference between the zones, with station 4A having a slightly higher annual average of 0.19 ± 0.14 μmol L^{-1} (Figure 3b). Throughout the study period, there was a uniform pattern of distribution for ammonia (NH_4^+), with station 4A recording a comparatively higher annual average value of 0.61 ± 0.38 μmol L^{-1} (Figure 3c). Like ammonia, phosphate (PO_4^{3-}) also exhibited constant concentrations throughout the region, ranging from an annual average of 0.08 ± 0.02 μmol L^{-1} to 0.15 ± 0.07 μmol L^{-1} (Figure 3c). In the case of silicate (SiO_4^{4-}) concentrations, the central zone witnessed slightly higher values than the other two zones, with the highest average values reported from station 3B (2.01 ± 0.41 μmol L^{-1}). Station 1B in the northern zone recorded the lowest average silicate values (1.17 ± 0.27 μmol L^{-1}) for the study period (Figure 3e).

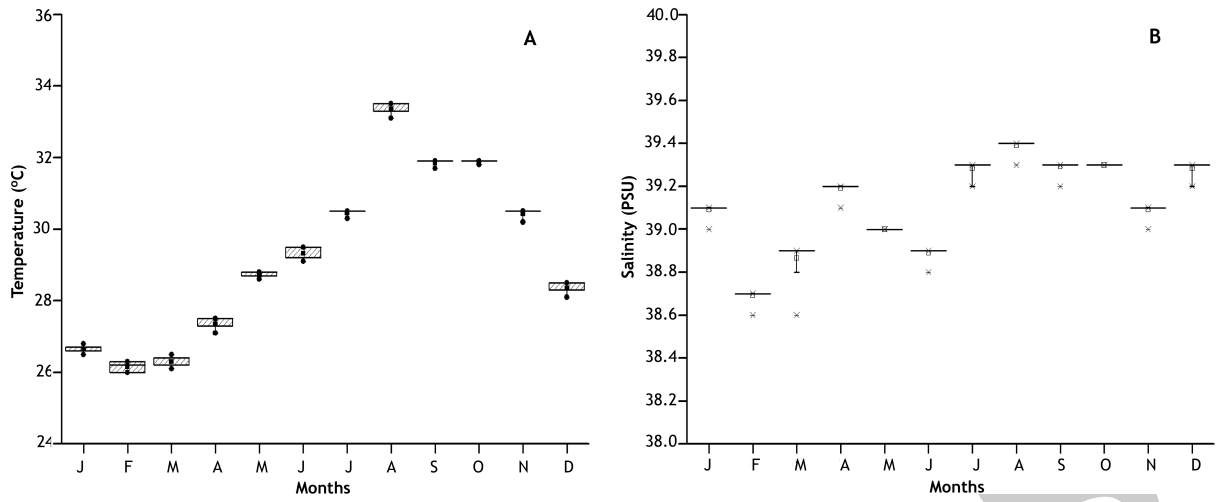

Figure 2. Monthly variations in physical parameters: temperature (A) and salinity (B) observed in the study region. Boxplots show the interquartile range (25th to 75th percentiles), with the median represented by a horizontal line and the mean indicated by a black dot. Whiskers extend to the minimum and maximum values within each sector, and error bars illustrate the variability across stations.

The SPM during the study period varied between annual averages of 1.28 ± 1.71 mg L^{-1} (4B) and 2.96 ± 2.25 mg L^{-1} with the central and southern zones depicting slightly higher values than the northern zone (Figure 3f). The spatiotemporal patterns of nutrient ratios revealed pronounced seasonal shifts in nutrient balance across the study area (Supplementary Table 1). N:P ratios were generally moderate during winter and spring (5–10) but declined sharply in June–July at several inner stations. In contrast, late summer (August–September) showed elevated N:P values across many sites, and isolated extreme peaks in November and December. Si:N ratios followed a complementary seasonal pattern; most stations exhibited low to moderate values (1–3) through much of the year, but a marked increase occurred in June–July, with several stations exceeding Si:N >5–10. Ratios declined again during August–September, reaching some of the lowest values (<1.5) (Supplementary Table 1).

3.3 Phytoplankton biomass (chlorophyll *a*)

The central zone stations consistently displayed higher phytoplankton biomass in terms of chlorophyll *a* concentrations. The annual average chlorophyll *a* values for the central zone stations varied between 0.55 ± 0.18 mg m^{-3} (station 3A) and 0.61 ± 0.30 mg m^{-3} (station 4A), with the highest concentration (1.54 mg m^{-3}) recorded from station 4B during October (Figure 4). The annual average chlorophyll *a* values for the northern zone ranged between 0.23 ± 0.12 mg m^{-3} (station 1A) and 0.32 ± 0.24 mg m^{-3} (station 2A) with the highest (0.89 mg m^{-3}) being observed from station 2A in July. The southern zone displayed an annual average chlorophyll *a* values that ranged between 0.25 ± 0.14 and 0.34 ± 0.16 mg m^{-3} at stations 5A and 6A, respectively (Figure 4). The coastal stations showed higher values in most of the occasions than their offshore counterpart.

3.4 Phytoplankton density

3.4.1 Total phytoplankton density

The total phytoplankton density for the study period showed both spatial and temporal differences. The central zone stations displayed considerable differences in monthly densities in comparison with the other two zones. The peak density in the central zone was observed mainly during the summer months with the highest density for the entire study period was obtained from station 3A ($43{,}393 \times 10^3$ cells m^{-3}) in July (Figure 5a). The annual average values obtained for the central zone stations ranged between $2216 \pm 3305 \times 10^3$ and $4681 \pm 12265 \times 10^3$ cells m^{-3} at stations 5A and 3A, respectively. The total phytoplankton densities (annual average) obtained for the northern zone stations ranged between $1359 \pm 2489 \times 10^3$ cells m^{-3} at station 1A and $1929 \pm 4265 \times 10^3$ cells m^{-3} at station 2B with the highest density of 14254×10^3 cells m^{-3} at station 2B in July (Figure 5a). Southern zone stations were the least prominent in terms of phytoplankton densities with annual averages ranging between $553 \pm 900 \times 10^3$ and $899 \pm 1283 \times 10^3$ cells m^{-3} at stations 6A and 5B, respectively. The highest total phytoplankton density from the southern zone was obtained from station 5B (4369×10^3 cells m^{-3}) during July (Figure 5a).

3.4.2 Centric diatom density

Spatially, centric diatoms showed considerable variation. The highest average value for this particular group of diatoms was observed at station 3A ($4209.22 \pm 12360.09 \times 10^3$ cells m^{-3}), followed by station 4A ($2077.55 \pm 4441.65 \times 10^3$ cells m^{-3}) and 3B ($2031.98 \pm 4955.45 \times$

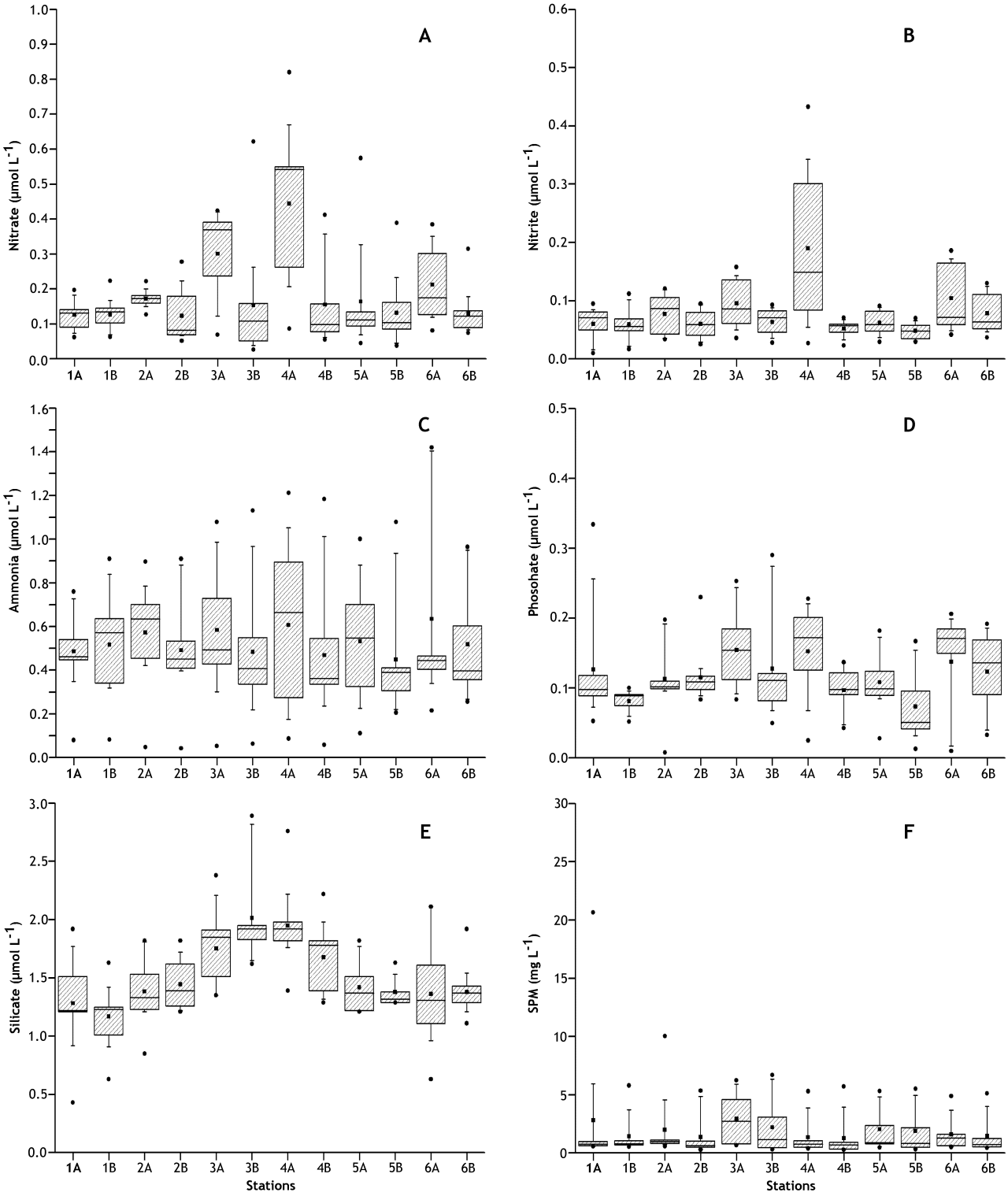

Figure 3. Concentrations of inorganic nutrient salts and suspended particulate matter (SPM) recorded during the study period across various stations. Boxplots display the interquartile range (25th to 75th percentiles), with the median shown as a horizontal line and the mean indicated by a black dot. Whiskers represent the minimum and maximum values, and error bars illustrate variability across stations.

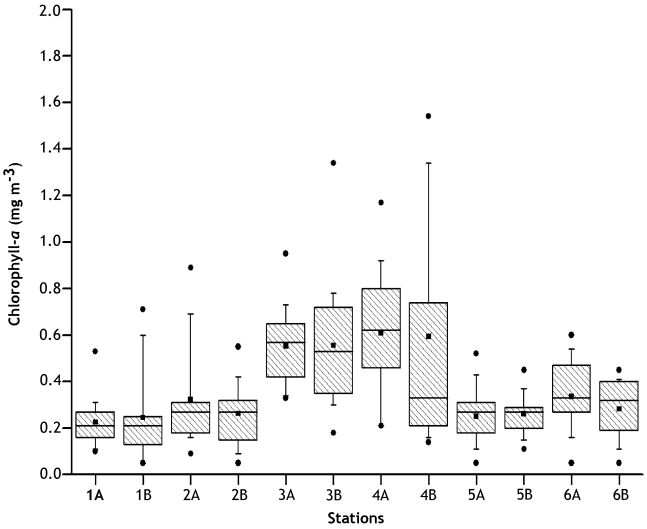

Figure 4. Spatial and temporal variations in chlorophyll *a* concentration, across different stations during the study period. Boxplots display the interquartile range (25th to 75th percentiles), with the median indicated by a horizontal line and the mean shown as a black dot. Whiskers extend to the minimum and maximum values, and error bars illustrate variability across stations.

10^3 cells m^{-3}), all of which are in the central zone of the study area (Figure 5b). In contrast, the lowest average values were observed at the southern zone stations, such as 6B ($408.22 \pm 859.49 \times 10^3$ cells m^{-3}) and 6A ($413.87 \pm 864.37 \times 10^3$ cells m^{-3}). Temporally, the summer months of July ($10158.54 \pm 11355.39 \times 10^3$ cells m^{-3}) and June ($4086.36 \pm 4035.54 \times 10^3$ cells m^{-3}) showed peak centric diatom densities, while May had the lowest average ($79.68 \pm 71.67 \times 10^3$ cells m^{-3}) for the entire study area. During the entire study period, the highest density was observed at station 3A (43334×10^3 cells m^{-3}) during July, and the lowest density was observed at station 3B (2×10^3 cells m^{-3}) during February (Figure 5b). The centric diatom species *Proboscia alata* (Brightwell) Sundström, 1986, made a substantial contribution to both total phytoplankton density and centric diatom abundance across the study area, particularly at the central zone stations (stations 3 and 4) (Figure 6a). This species exhibited a pronounced abundance during June and July, with the highest recorded density for the entire study observed at station 3A in July (43247×10^3 cells m^{-3}), and a corresponding spatial average of $9998 \pm 11{,}376 \times 10^3$ cells m^{-3}. In June, peak density was observed at station 4A (13062×10^3 cells m^{-3}), with a spatial average of $3915 \pm 3872 \times 10^3$ cells m^{-3}.

3.4.3 Pennate diatom density

Pennate diatoms also exhibited considerable spatial and temporal variations during the study period. Spatially, the highest average values were observed at station 4B ($881.85 \pm 1970.85 \times 10^3$ cells m^{-3}) and station 4A ($492.46 \pm 1146.44 \times 10^3$ cells m^{-3}), both of which are located in the central zone of the study region (Figure 5c). In contrast, the lowest average values were reported at station 2B ($29.86 \pm 29.57 \times 10^3$ cells m^{-3}) in the northern zone, and at station 6B ($33.60 \pm 29.56 \times 10^3$ cells m^{-3}) in the southern zone. Temporally, the highest abundance was reported in May ($1314.42 \pm 1883.85 \times 10^3$ cells m^{-3}), while the lowest of $14.24 \pm 14.70 \times 10^3$ cells m^{-3} was observed in April. The highest individual abundance was observed at station 3B (4597.41×10^3 cells m^{-3}) in May, and these diatoms were absent from many stations during various periods of the study (Figure 5c). The pennate diatom species *Lioloma elongatum* (Grunow) Hasle, 1997, emerged as a distinct and dominant taxon during May (Figure 6b). It was the primary contributor to total phytoplankton abundance in the central zone stations during this period. The species exhibited peak densities of 4.579×10^3 cells m^{-3} at station 3B and 4049×10^3 cells m^{-3} at station 4A, significantly influencing the overall phytoplankton abundance for that month.

3.4.4 Dinoflagellate density

Similar to diatoms, the presence of dinoflagellates also fluctuated in the different months and across various stations. Regarding spatial variation, the highest mean densities were detected at stations 4A ($278.89 \pm 322.47 \times 10^3$ cells m^{-3}) and 2B ($255.83 \pm 352.63 \times 10^3$ cells m^{-3}), which were only a little bit lower. On the contrary, the minimum occurrences were recorded at stations 6A ($72.57 \pm 76.77 \times 10^3$ cells m^{-3}) and 6B ($87.57 \pm 67.86 \times 10^3$ cells m^{-3}) (Figure 5d). Regarding temporal variation, the maximum number of dinoflagellates was observed in June ($481.13 \pm 349.93 \times 10^3$ cells m^{-3}), whereas the minimum was noted in March ($34.44 \pm 21.06 \times 10^3$ cells m^{-3}). The maximum density throughout the entire study was recorded in June at station 4A (1246×10^3 cells m^{-3}), whereas the minimum was observed at station 1A (5.96×10^3 cells m^{-3}) in January (Figure 5d).

3.4.5 Cyanophyte density

The cyanophyte population was the least prevalent phytoplanktonic community, with significant differences between locations and months of the year. The highest average density was reported in station 2B ($280.83 \pm 457.65 \times 10^3$ cells m^{-3}), whereas the lowest was seen in station 2A ($36.36 \pm 61.34 \times 10^3$ cells m^{-3}) (Figure 5e). On a seasonal basis, the highest densities were registered in November ($581.29 \pm 408.68 \times 10^3$ cells m^{-3}), while in March the lowest ones took place ($0.57 \pm 1.66 \times 10^3$ cells m^{-3}). The peak number (1329×10^3 cells m^{-3}) was counted at station 1B in July. This group of phytoplankton was also not captured at many locations and seasons in the study.

3.5 Phytoplankton diversity

In this study, a total of 284 different phytoplankton species were observed, encompassing four major groups: centric

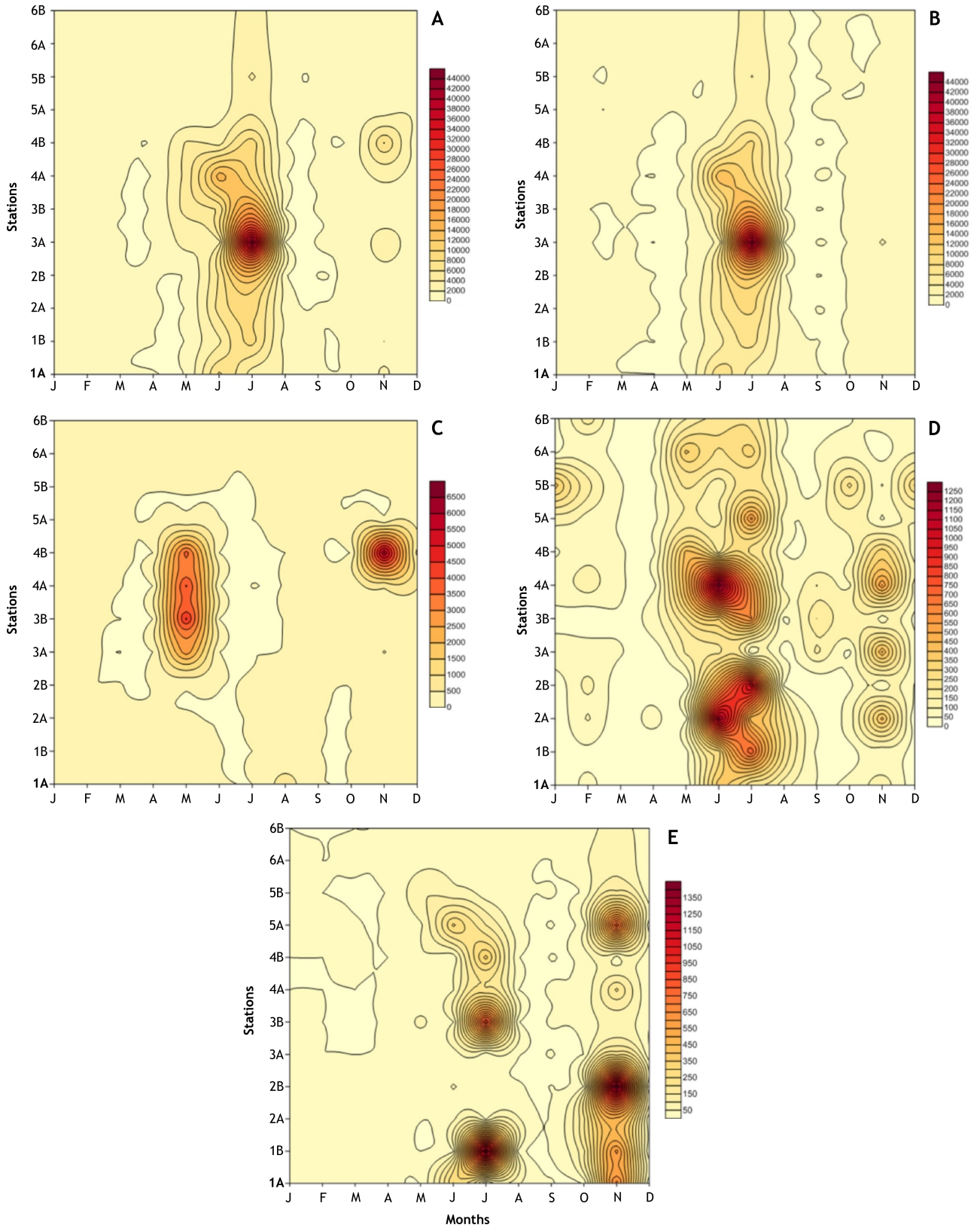

Figure 5. Surfer plots illustrating the spatiotemporal variations in total phytoplankton density (A) and group-specific abundances (B–E), including centric diatoms (B), pennate diatoms (C), dinoflagellates (D) , and cyanophytes (E), across the study region. Colour gradients represent density ranges for each group.

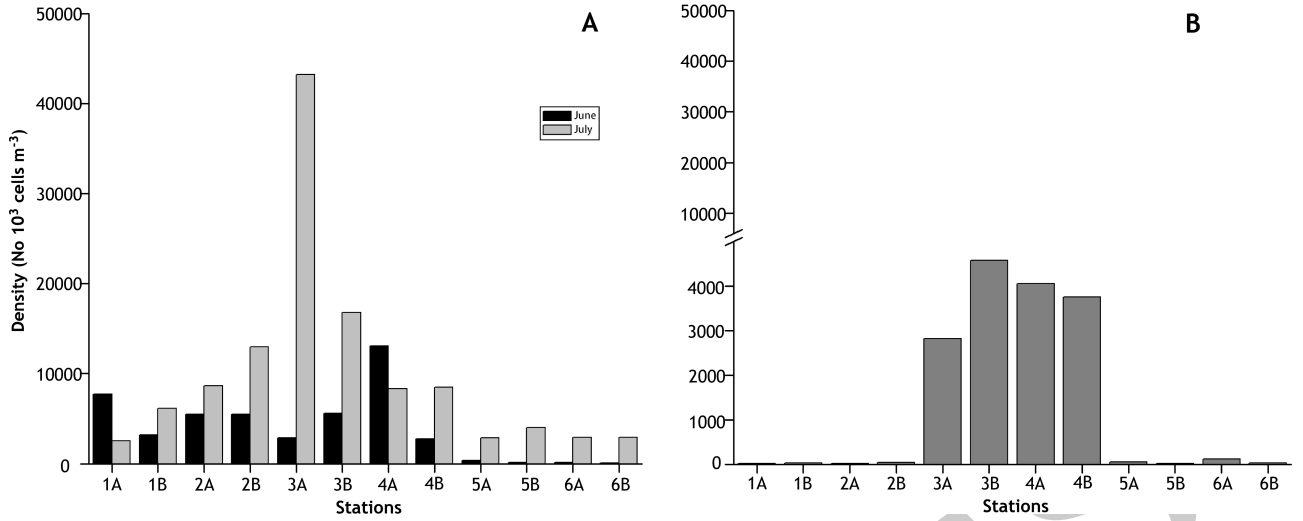

Figure 6. Distribution patterns of dominant diatom species across the study stations: *Proboscia alata* (Brightwell) Sundström, 1986 (A), a centric diatom, during June and July; and *Lioloma elongatum* (Grunow) Hasle, 1997 (B), a pennate diatom, during May.

diatoms, pennate diatoms, dinoflagellates, and cyanophytes (Supplementary Table 2). Diatoms, combining both centric and pennate forms, constituted the most diverse group with 150 species, representing approximately 53.3% of the total phytoplankton diversity. Centric diatoms alone contributed 100 species (35%), while pennate diatoms accounted for 50 species (18%). Dinoflagellates were also highly diverse, with 132 different species, making up 46% of the total diversity. Cyanophytes showed the least representation, with only two species observed (0.7%).

Among the centric diatoms, the genus *Chaetoceros* was the most speciose, contributing 34 species. It was followed by *Rhizosolenia* (19 species), *Guinardia* (4 species), and *Hemiaulus* (4 species) (Figure 7). These four genera collectively accounted for approximately 62% of the total centric diatom species richness. Within the pennate diatom category, *Pseudo-nitzschia* was the most dominant genus, contributing 8 species. *Thalassionema* and *Pleurosigma* contributed equally, with 4 species each (Figure 7). Collectively, these three genera comprised 33% of the total pennate diatom species observed. Dinoflagellates exhibited the greatest genus-level diversity, with *Tripos* contributing the highest number of species (37 species). It was followed by *Protoperidinium* (26 species), *Dinophysis* (11 species), *Prorocentrum* (7 species), *Phalacroma* (6 species), and *Gonyaulax* (5 species) (Figure 7). These six genera collectively represented approximately 69% of the total dinoflagellate diversity. *Trichodesmium* was the sole representative of the cyanophytes, with two species observed in this category (Figure 7).

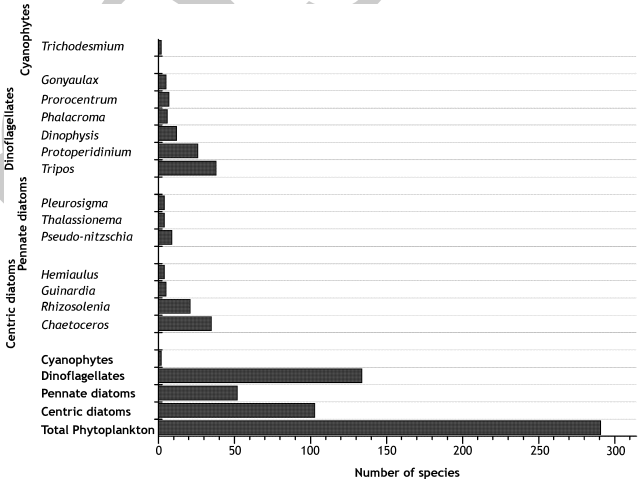

Figure 7. Phytoplankton diversity observed during the study period, illustrating the total number of species recorded and highlighting the most common genera within each major phytoplankton group from the coastal waters of Jeddah, Saudi Arabia.

3.5.1 Harmful algal bloom-causing species

Among the identified phytoplankton, 35 species were classified as harmful. This group was further divided into 20 harmful toxic species and 15 nontoxic but harmful species (Table 1). Dinoflagellates predominated the harmful toxic category, featuring genera such as *Dinophysis* (5 species), *Prorocentrum* (4 species), *Alexandrium*, *Gonyaulax*, *Karenia*, *Phalacroma* (3 species), and *Protoperidinium*. Additionally, four species of the diatom genus *Pseudo-nitzschia*, known producers of the neurotoxin domoic acid, were recorded. The harmful nontoxic group primarily consisted of diatoms, notably four species from the genus *Chaetoceros*, alongside *Cerataulina*, *Eucampia*, and four species from *Tripos*. Dinoflagellates like *Gonyaulax polygramma*, *Noctiluca scintillans*, and *Protoperidinium depressum* were

Table 1. Harmful phytoplankton species documented in the current study.

Toxic harmful species	Non-toxic harmful species
Pseudo-nitzschia australis Frenguelli, 1939	*Cerataulina pelagica* (Cleve) Hendey, 1937
Pseudo-nitzschia cuspidata (Hasle) Hasle, 1993	*Chaetoceros concavicornis* Mangin, 1917
Pseudo-nitzschia delicatissima (Cleve) Heiden, 1928	*Chaetoceros convolutus* Castracane, 1886
Pseudo-nitzschia seriata (Cleve) H.Peragallo, 1899	*Chaetoceros debilis* Cleve, 1894 emend Xu, Y. Li & Lundholm in Xu et al., 2020
Alexandrium affine (H. Inoue & Y. Fukuyo) Balech, 1995	*Chaetoceros tenuissimus* Meunier, 1913
Alexandrium minutum Halim, 1960	*Chaetoceros wighamii* Brightwell, 1856
Alexandrium tamarense (Lebour, 1925) Balech, 1995	*Eucampia zodiacus* Ehrenberg, 1839
Dinophysis acuminata Claparède & Lachmann, 1859	*Gonyaulax polygramma* Stein, 1883
Dinophysis acuta Ehrenberg, 1839	*Noctiluca scintillans* (Macartney) Kofoid & Swezy, 1921
Dinophysis caudata Saville-Kent, 1881	*Prorocentrum micans* Ehrenberg, 1834
Dinophysis miles Cleve, 1900	*Protoperidinium depressum* (Bailey, 1854) Balech, 1974
Dinophysis tripos Gourret, 1883	*Tripos dens* (Ostenfeld & Johannes Schmidt) F. Gómez, 2013
Gonyaulax spinifera (Claparède & Lachmann) Diesing, 1866	*Tripos furca* (Ehrenberg) F. Gómez, 2013
Karenia mikimotoi (Miyake & Kominami ex Oda) Gert Hansen & Moestrup, 2000	*Tripos fusus* (Ehrenberg) F. Gómez 2013
Phalacroma mitra F. Schütt, 1895	*Tripos lineatus* (Ehrenberg) F. Gómez, 2013
Phalacroma rotundatum (Claparéde & Lachmann) Kofoid & Michener, 1911	
Prorocentrum cordatum (Ostenfeld) J.D. Dodge, 1976	
Prorocentrum lima (Ehrenberg) F. Stein, 1878	
Prorocentrum mexicanum Osorio-Tafall, 1942	
Protoceratium reticulatum (Claparède & Lachmann) Bütschli, 1885	

also observed within this nontoxic but harmful classification (Table 1).

3.6 Statistical analysis

3.6.1 Pearson's coefficient of correlation (r)

Pearson's coefficient of correlation (r) analysis between various physiochemical and biological parameters revealed several significant relationships (Figure 8). Chlorophyll a concentrations showed a positive correlation with total phytoplankton density ($r = 0.401, p < 0.01$). It also exhibited significant positive correlations with silicate concentrations ($r = 0.253, p < 0.01$) and temperature ($r = 0.194, p < 0.05$). Similar to chlorophyll a, both total phytoplankton density and centric diatom density displayed significant positive correlations with silicates, with correlation coefficients of $r = 0.269$ ($p < 0.01$) and $r = 0.273$ ($p < 0.01$), respectively. The inorganic phosphate also showed significant positive relationships with total phytoplankton density ($r = 0.207, p < 0.01$) and centric diatom density ($r = 0.217, p < 0.01$). Interestingly, ammonia demonstrated a significant negative correlation with total phytoplankton density ($r = -0.262, p < 0.01$), centric diatom density ($r = -0.250, p < 0.01$), and dinoflagellate density ($r = -0.249, p < 0.05$) (Figure 8).

3.6.2 One-way ANOVA

One-way ANOVA results indicated that most abiotic and biotic parameters exhibited significant temporal variation over the study period (Supplementary Table 3). Among the physical parameters, salinity and temperature showed highly significant monthly variation ($p < 0.001$), whereas their spatial variation was not statistically significant ($p > 0.05$). Within the inorganic nutrients, nitrite displayed highly significant variation both spatially and temporally ($p < 0.001$). Ammonia varied significantly across months ($p < 0.001$) but showed no significant spatial variation. In contrast, nitrate showed strong spatial variation ($p < 0.001$) and moderate temporal variation ($p < 0.01$). Phosphate concentrations varied significantly across months ($p < 0.001$), while silicates exhibited significant variation among stations ($p < 0.001$). Phytoplankton biomass, represented by chlorophyll a, showed significant variation both spatially ($p < 0.001$) and temporally ($p < 0.05$). Similarly, total phytoplankton density and the densities of various phytoplankton groups showed significant temporal variation ($p < 0.001$), whereas spatial differences were not statistically significant ($p > 0.05$).

3.6.3 One-way ANOSIM (β-diversity)

One-way ANOSIM analysis revealed that the phytoplankton community structure across the six transects was significantly different during most months (Supplementary Table 4). Spatial variation in community composition was most pronounced in January and May ($p = 0.001$), indicating strong differentiation among transects during these periods. In contrast, the least spatial variation was observed in April ($p = 0.084$) and July ($p = 0.432$), suggesting a more homogeneous phytoplankton distribution during these months. Supplementary Table 5a–b provides detailed results of the pairwise test for each month.

3.6.4 t-test analysis

Since phytoplankton biomass and the abundance of most phytoplankton groups were markedly higher at stations 3 and 4, the variability in abiotic factors between these and the other stations was examined through a t-test. Among the physical variables, salinity and temperature did not show any significant differences (Supplementary Table 6). Similarly, SPM showed no significant variation between the two station groups. Interestingly, with the exception of

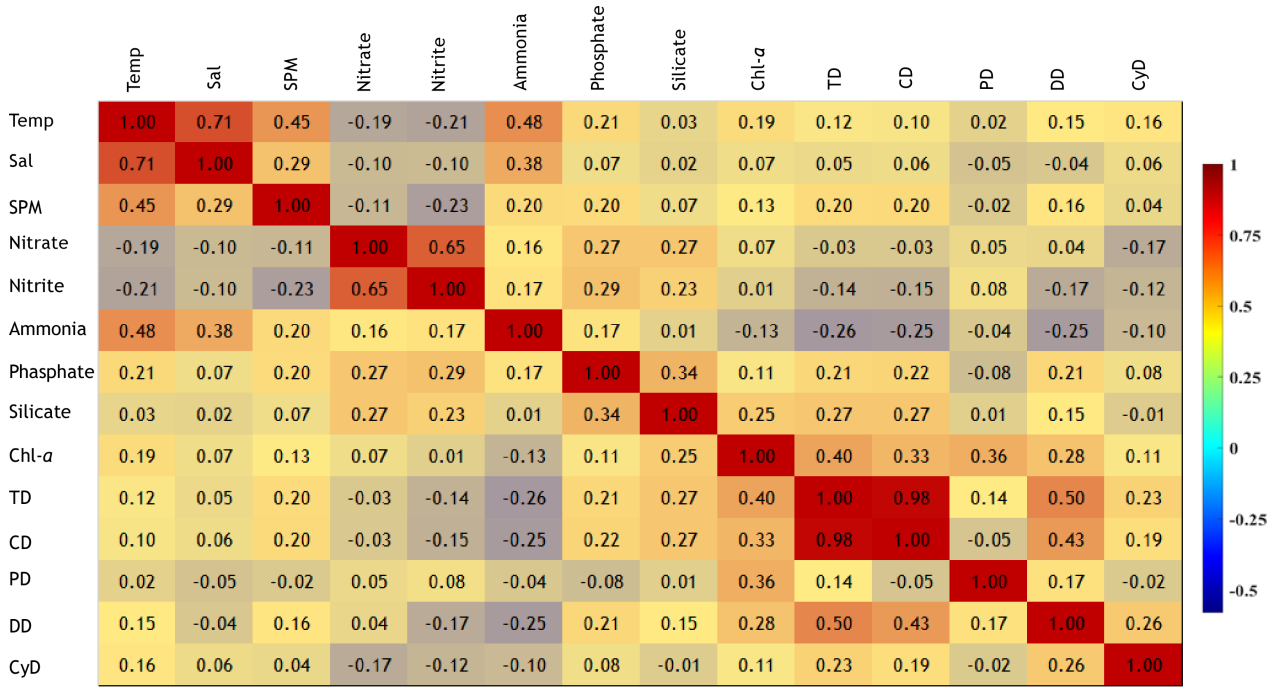

Figure 8. Pearson's correlation coefficients (r) matrix between biotic and abiotic parameters observed in the study. (TD = Total density, CD = centric diatom density, PD = Pennate diatom density, DD = Dinoflagellate density, CyD = cyanophyte density).

ammonia, all other nutrients – nitrate ($p < 0.0001$), nitrite ($p = 0.0039$), phosphate ($p = 0.0318$), and silicate ($p < 0.0001$) – showed significant differences between stations 3 and 4 and the other stations.

3.6.5 BIO-ENV analysis

The results of the BIO-ENV analysis indicated that the combination of nitrate, ammonia, phosphate, silicate, and SPM formed the most influential set of environmental variables, showing the highest correlation ($r = 0.993$) with the variability in phytoplankton community abundance (Supplementary Table 7). The second-best explanatory combination included SPM, nitrate, nitrite, ammonia, and phosphate, also demonstrating a strong association with the observed community patterns. The RDA triplot illustrated the environmental preferences of different phytoplankton groups (Figure 9). The first two axes explained 76.3% and 12.1% of variance. Phytoplankton biomass (chlorophyll *a*), total density, and the densities of centric diatoms, dinoflagellates, and cyanophytes were positively correlated with SPM, silicate, salinity, and phosphorus. In contrast, pennate diatom density showed a positive correlation with ammonia, nitrate, and nitrite (Figure 9).

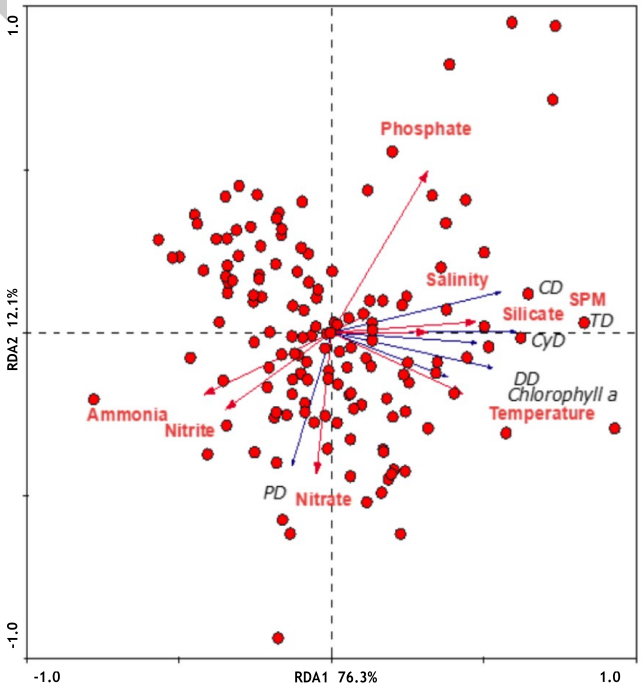

Figure 9. Redundancy Analysis (RDA) triplot illustrating the relationships between response variables (blue arrows) and explanatory variables (red arrows).

3.6.6 Biodiversity indices

Phytoplankton diversity, evaluated using species number (S), Margalef's richness index (D), Pielou's evenness (J'), and Shannon-Weiner diversity index (H'), showed distinct spatial patterns across the study area (Figure 10a–d). In the northern zone (stations 1 and 2), species numbers ranged from 27.6 to 31.8, with relatively low richness val-

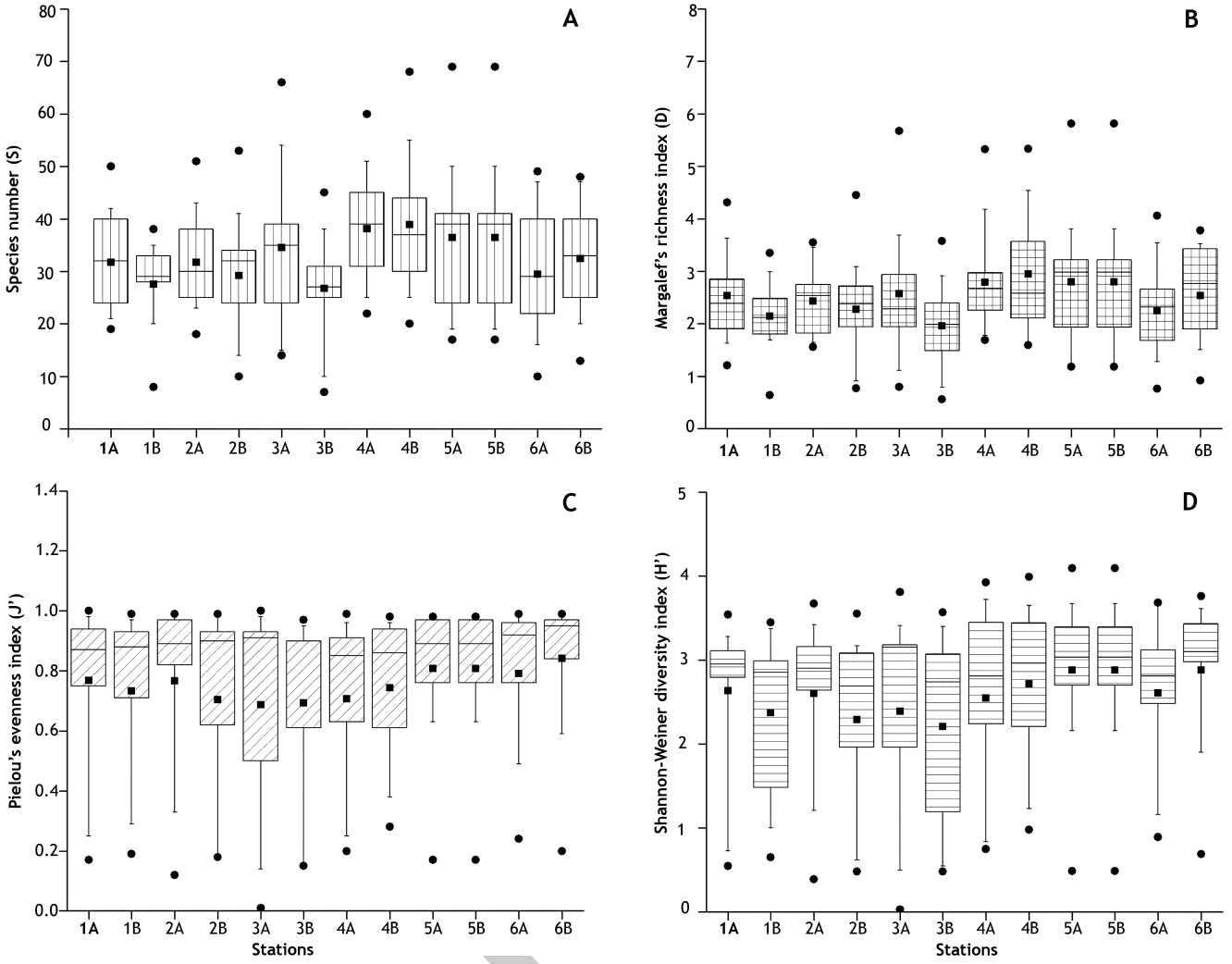

Figure 10. Variation in phytoplankton diversity metrics across sampling stations. (A) Species number, (B) Margalef's Richness Index, (C) Pielou's Evenness Index, and (D) Shannon-Wiener Diversity Index. Boxplots show the interquartile range (25th–75th percentiles); the horizontal line indicates the median, black dots represent the mean, and whiskers extend to the minimum and maximum values.

ues ($D = 2.19$–2.58) and moderate evenness (J' up to 0.81), resulting in Shannon diversity values between 2.3 and 2.5. The central zone (stations 3 and 4) exhibited a wider range of variability: While stations 4A and 4B recorded the highest species counts (38.1 and 38.9, respectively) and richness values above 3.0, station 3B showed the lowest diversity across all indices, including $S = 26.8$, $D = 2.20$, $J' = 0.53$, and $H' = 1.20$. These central stations also demonstrated strong temporal fluctuations, with particularly low evenness during June and July. In contrast, the southern zone (stations 5 and 6) had consistently higher and more stable diversity metrics. Species numbers exceeded 32 at all stations, with D values around 2.9–3.1, high evenness ($J' \geq 0.83$ at stations 6A and 6B), and the highest Shannon index recorded at station 6A ($H' = 3.19$) (Figure 10a–d).

4. Discussion

This study explored the seasonal and spatial variations of phytoplankton communities in Jeddah's coastal waters, highlighting significant changes in species composition and abundance across different regions and time frames. Notably, anthropogenic influences emerged as a key driver shaping phytoplankton dynamics, particularly in the central region of the study area. This zone, characterized by substantial human activity – including inputs from desalination plants, sewage discharge, and other coastal developments – exhibited pronounced alterations in community structure and elevated phytoplankton proliferation. We acknowledge the mesh-size bias associated with the 20-μm net, which selectively samples microphytoplankton while largely excluding pico- and nanophytoplankton. Given that the oligotrophic Red Sea is characteristically dominated by

picophytoplankton, the present dataset reflects only the microphytoplankton fraction of the community. Accordingly, all interpretations are made at the microphytoplankton group level, with this methodological limitation taken into account.

The physical parameters recorded in the study area largely followed the typical patterns characteristic of the central Red Sea and were consistent with previous observations reported for the coastal waters of Jeddah (Aziz et al., 2011; Al-Amri et al., 2020; El-Sherbiny et al., 2021). Salinity revealed minimal variation across the different sampling stations, with only slight temporal fluctuations observed between months. This consistency suggests a lack of significant external freshwater inputs capable of altering the prevailing salinity regime in the study area (Sofianos et al., 2002). In the present study, salinity exerted minimal influence on phytoplankton abundance and diversity, likely due to the long-term adaptation of native species to the naturally high-salinity conditions of the Red Sea, as previously noted by Devassy et al. (2017). As the region is characterized by naturally elevated and relatively stable salinity levels, the resident phytoplankton communities are well acclimated, exhibiting resilience to minor fluctuations within this salinity range (Al-Amri et al., 2020). In contrast to salinity, temperature exhibited significant temporal variation throughout the study period and had a notable impact on phytoplankton dynamics. A positive correlation was observed between temperature and phytoplankton biomass (as chlorophyll *a*). This relationship suggests that, when other environmental conditions – particularly the availability of inorganic nutrients – are favorable, temperature plays a key role in regulating phytoplankton proliferation in the Red Sea. Similar findings were reported by Devassy et al. (2017) in the northern Red Sea. This effect was especially pronounced in the central zone of the study area, where elevated levels of inorganic nutrients coincided with increased phytoplankton abundance and biomass. Previous studies in the Red Sea have also highlighted the importance of favorable temperature conditions in supporting the successful proliferation of phytoplankton, particularly diatoms (Al-Amri et al., 2020; El-Sherbiny et al., 2021). The observed phytoplankton proliferation, particularly in the central zone where anthropogenic pressures are most evident, underscores the critical influence of multiple environmental parameters in regulating phytoplankton growth in the Red Sea.

Inorganic nutrients exhibited low concentrations throughout most of the region, with the exception of the central zone, where elevated levels suggest localized enrichment resulting from sustained anthropogenic influences (Peña-García et al., 2014; Peña-García, 2022). The observed significant positive correlation between phosphate levels and total phytoplankton abundance highlights the importance of phosphorus as a limiting nutrient, reinforcing its key role in regulating primary productivity in the studied coastal waters (Fahmy, 2003; Al-Farawati et al., 2008). The central zone exhibited significantly higher concentrations of nitrates and silicates compared to the northern and southern stations indicating statistically meaningful spatial differences in nutrient distribution. This localized nutrient enrichment strongly indicates the persistent influence of anthropogenic activities, such as domestic wastewater discharge, industrial effluents, and coastal development (Al-Farawati et al., 2018; Peña-García et al., 2014). In contrast, the relatively low nutrient levels in other zones reflect more oligotrophic conditions, typical of the Red Sea. The spatial disparity in nutrient availability suggests that human-induced inputs are a key driver of biogeochemical variability in the central region, potentially altering phytoplankton dynamics and ecosystem functioning. This particular region, along with several nearby coastal lagoons such as Al-Arbaeen and Al-Shabab, has historically received substantial nutrient inputs (Ba-Akdah et al., 2008; El Sayed et al., 2011). Over the past two decades, the rate of nutrient loading has increased significantly, leading to the development of severe eutrophication problems (El Sayed, 2002; Ewea, 2010; Turki and Mudarris, 2008). Recent studies have documented eutrophication in these lagoons, highlighting the detrimental impacts of excessive nutrient enrichment (Ghandourah et al., 2023; Orif et al., 2023). As a result, the surrounding coastal ecosystems have been increasingly degraded, with notable shifts in water quality, biological productivity, and ecological balance (El-Sherbiny et al., 2021; Peña-García, 2022). The central zone in the present study encompasses a densely populated urban area, characterized by substantial sewage discharge and the operation of a desalination plant (Peña-García et al., 2014; Cai et al., 2024). These factors likely contribute to the continuous input of nutrients into the coastal waters, leading to localized enrichment and influencing the observed patterns of phytoplankton proliferation in the current study. Discharge rates are likely higher during the summer months (Mudarris and Turki, 2006), which, when combined with favorable temperature conditions, may have contributed to the observed phytoplankton proliferation during this period. Currently, the influence of such discharges, particularly in the central zone extends up to 4 km from the shore, as evidenced by their impact on the offshore stations studied. This offshore dispersal of nutrient-rich effluents poses a significant risk to the broader marine ecosystem, potentially leading to shifts in community structure, oxygen depletion, and long-term degradation of water quality (Ansari et al., 2011; Dorgham, 2014). In contrast to the northern and southern zones, the central zone displays a distinct nutrient–phytoplankton interaction pattern, likely driven by consistent anthropogenic inputs and localized environmental conditions. Statistical analysis (*t*-test) of the central zone stations indicated that, with the exception of ammonia, all measured nutrients – particularly nitrates, phosphates, and silicates –

exhibited significant positive correlations with phytoplankton abundance ($p < 0.05$). This suggests that phytoplankton proliferation in this zone is closely linked to nutrient availability. Although currently observed as a localized phenomenon, the sustained nutrient enrichment possesses the potential to escalate, leading to broader eutrophication of the coastal system and increasing the risk of HAB outbreaks (Smayda, 2008; Glibert et al., 2018). Similar events have previously been reported in the coastal waters of Jeddah (Al-Aidaroos et al., 2019) underscoring the vulnerability of the region to such ecological disturbances. The northern zone, characterized by minimal human activity and the absence of external inputs, continues to serve as a reference site representing relatively pristine environmental conditions in the region. In contrast, the southern zone – despite the presence of potential sources of anthropogenic input such as an international seaport and a sewage treatment plant – did not exhibit nutrient levels comparable to those of the central zone. This discrepancy may be attributed to the prevailing hydrodynamic conditions in the southern region, which likely facilitate the dispersion or dilution of nutrient inputs (Basaham et al., 2009; Al-Barakati et al., 2011). The current-driven flushing could either mitigate the localized impact or transport the effluents away from the sampling area, thereby reducing their influence on observed nutrient concentrations and biological responses. In the current study, the variability observed in N:P and Si:N ratios further supports the influence of localized anthropogenic nutrient enrichment in shaping phytoplankton dynamics, particularly in the central zone where sustained inputs alter the natural stoichiometric balance. These shifts in nutrient ratios indicate modified nutrient limitation patterns – periodically intensifying P or Si stress – which may reinforce the risk of phytoplankton proliferation and ecosystem imbalance already documented for this heavily impacted region. Phytoplankton biomass (as chlorophyll *a*) exhibited a similar spatial pattern to that of nutrient distribution across the study area. Except for the central zone stations, chlorophyll *a* levels remained relatively low, reflecting the oligotrophic characteristics of the Red Sea (Kürten et al. 2015; Kheireddine et al., 2017, 2021). In contrast, the central zone recorded significantly elevated chlorophyll *a* concentrations compared to the northern and southern zones, indicating a nutrient-enriched environment that supports enhanced phytoplankton growth and proliferation. This pattern aligns with observations from the limited number of studies (Khomayis, 2002; Al-Amri et al., 2020; El-Sherbiny et al., 2021) conducted in areas adjacent to the current study stations, which similarly reported higher phytoplankton productivity in response to localized nutrient enrichment. Statistical analyses revealed that spatial variation was more pronounced than temporal variation, highlighting the influence of localized nutrient enrichment in the study area. In the present study, chlorophyll *a* concentrations showed a significant positive correlation with temperature ($p < 0.05$), underscoring the role of ambient temperature in facilitating phytoplankton proliferation in the Red Sea. This relationship was particularly evident in the central zone, where chlorophyll *a* levels peaked during the summer months, suggesting that elevated temperatures, in combination with nutrient availability, create favorable conditions for phytoplankton growth. These findings are consistent with previous observations of summer-associated chlorophyll increases in various coastal regions of the Red Sea (Acker et al., 2008; Racault et al., 2015; Devassy et al., 2017), including the waters of Jeddah (Khomayis, 2002; El-Sherbiny et al., 2021). Additionally, Al-Amri et al. (2020) reported eutrophic-level chlorophyll *a* concentrations in several coastal lagoons within the region, indicating the recurrent nature of such events and reinforcing the susceptibility of these areas to nutrient-driven phytoplankton blooms.

Total phytoplankton abundance exhibited significant spatial and seasonal variability. Seasonal differences were more pronounced during the summer months ($p < 0.001$), particularly at the central zone stations. Although summer phytoplankton dominance was observed across all zones, the magnitude of proliferation in the central zone stations was particularly pronounced, representing the most distinct feature of the current study. Such temperature-driven phytoplankton proliferation, when supported by adequate nutrient availability, has been well documented in the coastal waters of the northern Red Sea by Devassy et al. (2017). Al-Amri et al. (2020) also reported a similar summer proliferation of phytoplankton in the coastal waters of Jeddah, particularly within several lagoon systems, highlighting the seasonal response of phytoplankton to elevated temperatures and nutrient availability. Outside the May–July period, phytoplankton abundance at the central zone stations was considerably lower, further suggesting a seasonal preference among dominant Red Sea phytoplankton for the summer months, when environmental conditions are more suitable for successful flourishing. The elevated phytoplankton abundance during this period may be attributed either to intensified anthropogenic inputs or to limited dispersion of these inputs due to prevailing hydrodynamic conditions (Al-Farawati et al., 2008; Peña-García, 2022; Peña-García et al., 2014). Further investigation is warranted to determine why nutrient enrichment appears to predominantly affect the central zone stations. It remains unclear whether this localized response is driven by unique hydrodynamic features – such as current circulation or wave patterns – that facilitate the retention and concentration of inorganic nutrients within this zone, thereby creating a more favorable environment for sustained phytoplankton proliferation. Collectively, the findings from previous studies, together with the results of the present investigation, underscore the susceptibility of Red Sea coastal regions to phytoplankton dominance under favorable environmental conditions, particularly during

periods of elevated temperature and nutrient enrichment.

As observed in the current study, a pronounced surge in diatom abundance during May–July at the central zone stations was primarily driven by the dominance of two species: the centric diatom *P. alata* and the pennate diatom *L. elongatum*. *Proboscia alata* exhibited continuous dominance over a 2-month period (June–July), reflecting its adaptation to the oligotrophic, warm waters of the Red Sea and supporting its classification as a native species of this region. Its dominance in other coastal areas of the Red Sea has been well documented, notably by Devassy et al. (2017), from the Al-Wajh region in the northern Red Sea. This evidence collectively confirms *P. alata* as an indigenous species with a strong capacity to thrive under the Red Sea's challenging environmental conditions (Post et al., 2002; Kürten et al., 2015). Further experimental studies examining the response of *P. alata* to increasing water temperatures would be valuable, as this species may serve as a key indicator or dominant phytoplankton taxon under future global warming scenarios. Its demonstrated resilience suggests it could potentially thrive and dominate in progressively warmer ocean conditions. The relative absence or lower abundance of *P. alata* during other months and at different stations suggests that this species can persist under unfavorable conditions and subsequently proliferate when environmental conditions become favorable. Whether its dominance exerts beneficial or detrimental effects on the coastal ecosystem can only be determined through continuous and long-term monitoring of the Red Sea's coastal waters. Centric diatom dominance within the phytoplankton community is a common feature in the coastal waters, as reported by Al-Amri et al. (2020) in their studies of two coastal lagoons in Jeddah. Their findings highlighted *Skeletonema costatum* and *Chaetoceros decipiens* as the dominant centric diatom species, further supporting the prevalence of centric taxa in nutrient-enriched, nearshore environments. The pennate diatom *L. elongatum* exhibited notable dominance during May, particularly across stations within the central zone. This indicates that pennate diatoms, like their centric counterparts, are capable of thriving under favorable environmental conditions. Similar patterns of pennate diatom dominance have been previously reported in the coastal waters of the Red Sea by Devassy et al. (2017) and El-Sherbiny et al. (2021), further supporting their ecological relevance and adaptive success in this region. Dinoflagellates exhibited a relatively uniform distribution in terms of abundance throughout the study period, reflecting a typical characteristic of the Red Sea phytoplankton community (Ismael, 2015; Kürten et al., 2015; Devassy et al., 2017). No distinct proliferation events involving this group were observed, and their stable presence suggests that dinoflagellates maintain a consistent, background role in the region's coastal ecosystem under the prevailing environmental conditions (Al-Amri et al., 2020; El-Sherbiny et al., 2021). In contrast to earlier studies, cyanophyte abundance was relatively low in the present investigation. Although the filamentous cyanobacterium *Trichodesmium erythraeum* is known to proliferate during the summer months and often forms extensive bloom patches across the Red Sea, its occurrence in this study was limited to low concentrations, even during peak summer conditions. This reduced presence may be attributed to the proximity of the sampling stations to the coastal zone, as *Trichodesmium* is more commonly observed forming surface aggregations in offshore, open-water environments rather than nearshore areas (Post et al., 2002).

The phytoplankton community in the present study was dominated by diatoms, followed closely by dinoflagellates, which reflects the typical structure of Red Sea marine ecosystems (Ismael, 2015; Kürten et al., 2015; Devassy et al., 2017). In terms of abundance, diatoms consistently outnumbered dinoflagellates; however, with respect to species diversity, both groups exhibited comparable richness. In the study of Devassy et al. (2017), dinoflagellates even surpassed diatoms in diversity, highlighting the ecological complexity and variability within the phytoplankton community of the Red Sea. The Red Sea is traditionally recognized for its high biodiversity across various aquatic organisms (DiBattista et al., 2016), and the findings of the present study further substantiate this by revealing significant diversity within the phytoplankton community composition. Within the centric diatom community of the Red Sea, the genera *Chaetoceros* and *Rhizosolenia* are recognized as key contributors (Ismael, 2015; Kürten et al., 2015; Devassy et al., 2017), a pattern that was also evident in the present study. These genera were consistently dominant across stations, aligning with findings from previous research in the region (Al-Amri et al., 2020; El-Sherbiny et al., 2021). Their prevalence can be attributed to their notable adaptive capacity, enabling them to thrive under the extreme environmental conditions characteristic of the Red Sea, including high salinity and temperature. This ecological resilience supports their status as well-adapted and regionally established taxa. The Red Sea is increasingly regarded as a natural laboratory for studying future oceanic conditions under global warming scenarios, due to its inherently high temperatures, salinity, and oligotrophic nature (Berumen et al., 2019). In this context, the dominant and resilient phytoplankton species identified in this study, such as those from the genera *Chaetoceros* and *Rhizosolenia*, may serve as potential contributors to future global ocean productivity, given their demonstrated capacity to thrive under extreme environmental conditions. *Pseudo-nitzschia* emerged as a prominent representative of the pennate diatom group in the present study. This genus warrants particular attention, as several of its species are known to form HABs and produce domoic acid, a neurotoxin of concern for marine food webs and human health. Notably, a recent HAB event in the Jeddah region was at-

tributed to this genus (Al-Aidaroos et al., 2019), underscoring the need for continued monitoring and species-level identification to assess potential ecological and public health risks associated with *Pseudo-nitzschia* blooms in the Red Sea. Interestingly, none of the traditionally diverse diatom genera – such as *Chaetoceros* and *Rhizosolenia* – were responsible for the significant summer phytoplankton proliferation observed in the central zone stations. Instead, the bloom was dominated by two less commonly reported species: *P. alata* and *L. elongatum*. This highlights the importance of localized environmental conditions in shaping community composition and suggests that even highly diverse genera may not dominate under certain ecological scenarios. Although a previous study (Al-Amri et al., 2020) from the Jeddah region reported bloom-like events associated with *Chaetoceros*, the present findings emphasize that bloom formation in the Red Sea is not exclusively linked to the most diverse or historically dominant genera. The dinoflagellate genera *Tripos* and *Protoperidinium* constituted the majority of dinoflagellate diversity in the present study. These genera have long been recognized as dominant components of the Red Sea phytoplankton community, as documented in earlier studies (Kürten et al., 2015; Devassy et al., 2017; Al-Amri et al., 2020; El-Sherbiny et al., 2021). Their continued prevalence highlights their ecological adaptability and preference for the Red Sea's high-salinity, oligotrophic conditions. Although *Tripos* and *Protoperidinium* contributed significantly to dinoflagellate diversity, neither genus exhibited any notable proliferation during the study period. This further substantiates the characterization of the Red Sea as a diatom-dominated ecosystem, where dinoflagellates, while diverse, typically play a secondary role in terms of biomass and abundance (Kürten et al., 2015; Devassy et al., 2017). Cyanophytes, as expected, were represented by only two species and are considered endemic to the Red Sea, reflecting their adaptation to the region's unique environmental conditions (Post et al., 2002). Phytoplankton diversity, richness, and evenness showed clear spatial and temporal variation across the studied stations. Central and southern stations generally exhibited higher species diversity and more balanced community structures, particularly during the spring months, suggesting that the central region is ecologically distinct. This uniqueness is likely attributed to the availability of inorganic nutrient inputs, which support both elevated phytoplankton abundance and diversity. In contrast, lower diversity and evenness in some central stations suggest localized environmental stresses or dominance by a few taxa during certain periods. A few freshwater and brackish diatom taxa (e.g., *Asterionella formosa*, *Aulacoseira granulate* and *Fragilaria* spp.) were recorded in isolated samples. Their occurrence is considered allochthonous, most likely introduced episodically through sewage runoff, stormwater input, or land-based discharge into the study area. These taxa were present in very low abundance and did not influence the overall community structure, but their presence indicates occasional terrestrial influxes that may transport nonmarine microflora into the coastal system. Such incidental records are consistent with similar observations in nearshore environments subjected to variable anthropogenic inputs (Al-Amri et al., 2020; El-Sherbiny et al., 2021).

The occurrence of 40 HAB-forming phytoplankton species – comprising approximately 14% of the total community – raises a significant ecological concern for the region, aligning with previous findings from other parts of the Red Sea (Kürten et al., 2015; Devassy et al., 2017; Al-Amri et al., 2020; El-Sherbiny et al., 2021), and highlighting the growing risk of HAB events in this vulnerable coastal ecosystem. Notably, 21 of these species are known to be potentially toxic, underscoring the increasing risk to marine ecosystems and public health. These findings suggest that the traditionally oligotrophic nature of the Red Sea, particularly in its coastal regions, may be undergoing notable shifts, likely driven by localized anthropogenic pressures. Such nutrient enrichment can trigger coastal phytoplankton blooms, which, while indicative of elevated productivity, may also pose ecological risks by disrupting the natural balance of the ecosystem (Banguera-Hinestroza et al., 2016), thereby underscoring the importance of regular monitoring and the implementation of early warning systems (Gokul et al., 2020) to mitigate potential environmental impacts. Similar observations have been previously reported in the Red Sea, with studies by Al-Aidaroos et al. (2019) documenting a significant bloom of *P. delicatissima* in the coastal waters of Jeddah, further highlighting the region's vulnerability to HAB events. The presence of this potentially harmful species in the current study as well suggests that *P. delicatissima* may now be a regular component of the Red Sea phytoplankton community, likely sustained by changing environmental conditions. Therefore, continuous monitoring of coastal waters is essential for assessing and managing the health of marine ecosystems, particularly the ecologically sensitive and globally significant coral reef systems of the Red Sea.

Acknowledgements

This project was funded by the Deanship of Scientific Research (DSR) at King Abdulaziz University, Jeddah, Saudi Arabia, under the grant no. (IPP: 736-150-2025). The authors, therefore, acknowledge with thanks DSR for technical and financial support. We also sincerely thank Dr. Kusum Karati for his assistance with statistical analysis.

Supplementary material

Supplementary material associated with this article can be found here.

Conflict of interest

None declared.

References

Acker, J., Leptoukh, G., Shen, S., Zhu, T., Kempler, S., 2008. *Remotely-sensed chlorophyll a observations of the northern Red Sea indicate seasonal variability and influence of coastal reefs*. J. Mar. Syst. 69 (3–4), 191–204. https://doi.org/10.1016/j.jmarsys.2005.12.006

Al-Aidaroos, A.M., Devassy, R.P., El-Sherbiny, M.M., 2019. *Unusual dominance of harmful microalgae Pseudo-nitzschia delicatissima cf. (Cleve) Heiden in the coastal waters of Jeddah, central Red Sea*. Pak. J. Bot. 51 (2), 1–6. https://doi.org/10.30848/PJB2019-2(44)

Al-Amri, A.A., Qari, H.A., El-Sherbiny, M.M., 2020. *Distribution and community structure of microphytoplankton in relation to increasing anthropogenic impact along coastal waters of Jeddah, the central Red Sea*. Oceanol. Hydrobiol. Stud. 49 (2), 193–205. https://doi.org/10.1515/ohs-2020-0018

Al-Barakati, A.M., 2011. *A study of tidal water circulation using a two-dimensional model in Jeddah Islamic Port, Red Sea*. JKAU: Mar. Sci. 22, 113–123.

Al-Farawati, R., Al-Maradni, A., Niaz, R., 2008. *Chemical characteristics (nutrients, fecal sterols and polyaromatic hydrocarbons) of the surface waters for Sharm Obhur, Jeddah, Eastern Coast of the Red Sea*. JKAU: Mar. Sci. 19, 95–119.

Al-Farawati, R., El Sayed, M.A.K., Rasul, N.M., 2018. *Nitrogen, phosphorus and organic carbon in the Saudi Arabian Red Sea Coastal Waters: behaviour and human impact*. [In:] Rasul, N., Stewart, I. (Eds.) *Oceanographic and biological aspects of the Red Sea*, Springer Int. Publ., 89–104. https://doi.org/10.1007/978-3-319-99417-8_5

Al-Yamani, F., Saburova, M., Polikarpov, I., 2024. *A comparison of potentially harmful microalgae and phytoplankton blooms in the Arabian Gulf and the Red Sea*. [In:] Rasul, N.M., Stewart, I.C. (Eds.), *Coral reefs and associated marine fauna around the Arabian Peninsula*, CRC Press, 267–287. https://doi.org/10.1201/9781003321392-24

Anderson, M.J., Crist, T.O., Chase, J.M., Vellend, M., Inouye, B.D., Freestone, A.L., Sanders, N.J., Cornell, H.V., Comita, L.S., Davies, K.F., Harrison, S.P., Kraft, N.J.B., Stegen, J.C., Swenson, N.G., 2011. *Navigating the multiple meanings of β diversity: a roadmap for the practicing ecologist*. Ecol. Lett. 14 (1), 19–28. https://doi.org/10.1111/j.1461-0248.2010.01552.x

Ansari, A.A., Gill, S.S., Khan, F.A., 2011. *Eutrophication: threat to aquatic ecosystems*, [In:] Eutrophication: causes, consequences and control, Springer, Dordrecht, London, New York, 143–170. https://doi.org/10.1007/978-90-481-9625-8_7

Aziz, B.S.A., Kosaki, Y., Ishikawa, M., 2011. *Water environmental conditions in the Jeddah coast*. Mem. Osaka Inst. Technol. Ser. A, 56, 17–21.

Ba-Akdah, M.A., Radi, N.I., Jastania, H.A., 2008. *Determination of some micro-nutrient Salt concentrations of Al-Nawras lagoon surface waters at Jeddah coast on the Red Sea*. JKAU Mar. Sci. 19, 29. https://doi.org/10.4197/mar.19-1.3

Banguera-Hinestroza, E., Eikrem, W., Mansour, H., Solberg, I., Curdia, J., Holtermann, K., Edvardsen, B., Kaartvedt, S., 2016. *Seasonality and toxin production of Pyrodinium bahamense in a Red Sea lagoon*. Harmful Algae, 55, 163–171. https://doi.org/10.1016/j.hal.2016.03.002

Basaham, A.S., Rifaat, A.E., El-Mamoney, M.H., El Sayed, M.A., 2009. *Re-evaluation of the impact of sewage disposal on coastal sediments of the Southern Corniche, Jeddah, Saudi Arabia*. JKAU: Mar. Sci. 20, 109–126.

Berumen, M.L., Voolstra, Ch.R., Daffonchio, D., Agusti, S., Aranda, M., Irigoien, X., Jones, B.H., Morán, X.A.G., Duarte, C.M., 2019. The Red Sea: Environmental gradients shape a natural laboratory in a Nascent Ocean. [In:] Voolstra, C., Berumen, M. (Eds.), *Coral reefs of the Red Sea*, Springer, Cham, 1–10. https://doi.org/10.1007/978-3-030-05802-9_1

Cai, C., Devassy, R. P., El-Sherbiny, M. M., Agusti, S., 2024. *Influence of seasonal variation and anthropogenic activities on elemental compositions in zooplankton: a year-long case study from the Jeddah coast of the Red Sea*. Earth Syst. Environ. 8 (3), 627–643. https://doi.org/10.1007/s41748-024-00403-2

Carvalho, S., Kürten, B., Krokos, G., Hoteit, I., Ellis, J., 2019. *The Red Sea*. [In:] Sheppard, C. (Ed.) *World seas: An environmental evaluation*, Acad. Press, 49–74. https://doi.org/10.1016/B978-0-08-100853-9.00004-X

Cullen, J.J., 2008. *Observation and prediction of harmful algal blooms*. [In:] Babin, M., Roesler, C. S., Cullen, J. J. (Eds.), *Real-time coastal observing system for marine ecosystem dynamics and harmful algal blooms: theory, Instrument and Modeling*, Oceanogr. Method. Ser., UNESCO, Paris, 1–41.

Devassy, R.P., El-Sherbiny, M.M., Al-Sofyani, A.M., Al-Aidaroos, A.M., 2017. *Spatial variation in the phytoplankton standing stock and diversity in relation to the prevailing environmental conditions along the Saudi Arabian coast of the northern Red Sea*. Mar. Biodivers. 47, 995–1008. https://doi.org/10.1007/s12526-017-0693-4

DiBattista, J.D., Howard, C.J., Gaither, M.R., Hobbs, J.P.A., Lozano-Cortés, D.F., Myers, R.F., Paulay, G., Rocha, L.A., Toonen, R.J., Westneat, M.W., Berumen, M.L., 2016. *On the origin of endemic species in the Red Sea*. J. Biogeogr. 43 (1), 13–30. https://doi.org/10.1111/jbi.12631

Dorgham, M., 2014. *Effects of Eutrophication*. [In:] Ansari, A.A., Gill, S.S. (Eds.), *Eutrophication: Causes, Consequences and Control*. Springer, Dordrecht, 29–44. https://doi.org/10.1007/978-94-007-7814-6_3

Durkin, C.A., Van Mooy, B.A., Dyhrman, S.T., Buesseler, K.O., 2016. *Sinking phytoplankton associated with carbon flux in the Atlantic Ocean*. Limnol. Oceanogr. 61 (4), 1172–1187. https://doi.org/10.1002/lno.10253

El Sayed, M.A., 2002. *Distribution and behavior of dissolved species of nitrogen and phosphorus in two coastal Red Sea lagoons receiving domestic sewage*. JKAU: Mar. Sci. 13, 47–73.

El Sayed, M.A., El-Maradny, A.A., Al Farawati, R., Shaban, Y.A., 2011. *Evaluation of the adequacy of a rehabilitation programme, implemented in two Red Sea coastal lagoons, using the hydrological characteristics of surface water*. JKAU: Mar. Sci. 22 (2), 69–108. https://doi.org/10.4197/Mar.22-2.6

El-Sherbiny, M.M., Al-Harbi, M.A., Kumar, A.J., 2021. *Spatio-temporal variation of microphytoplankton communities in Obhur Creek, the central Red Sea*. Oceanol. Hydrobiol. Stud. 50 (1), 98–114. https://doi.org/10.2478/oandhs-2021-0010

Ewea, H.A., 2010. *Hydrological analysis of flooding wastewater lake in Jeddah, Saudi Arabia*. JKAU: Met. Env. Arid Land Agric. Sci. 21 (1), 125–144.

Fahmy, M., 2003. *Water quality in the Red Sea coastal waters (Egypt) analysis of spatial and temporal variability*. Chem. Ecol. 19 (1), 67–77. https://doi.org/10.1080/0275754031000087074

Falkowski, P.G., 1994. *The role of phytoplankton photosynthesis in global biogeochemical cycles*. Photosynth. Res. 39, 235–258. https://doi.org/10.1007/BF00014586

Ghandour, I.M., Basaham, S., Al-Washmi, A., Masuda, H., 2014. *Natural and anthropogenic controls on sediment composition of an arid coastal environment: Sharm Obhur, Red Sea, Saudi Arabia*. Environ. Monit. Assess. 186, 1465–1484. https://doi.org/10.1007/s10661-013-3467-x

Ghandourah, M.A., Orif, M.I., Al-Farawati, R.K., El-Shahawi, M.S., Abu-Zeid, R.H., 2023. *Illegal pollution loading accelerate the oxygen deficiency along the coastal lagoons of eastern Red Sea*. Reg. Stud. Mar. Sci. 63, 102982. https://doi.org/10.1016/j.rsma.2023.102982

Glibert, P.M., Al-Azri, A., Icarus Allen, J., Bouwman, A.F., Beusen, A.H., Burford, M.A., Harrison, P.J., Zhou, M., 2018. *Key questions and recent research advances on harmful algal blooms in relation to nutrients and eutrophication*. [In:] Glibert, P., Berdalet, E., Burford, M., Pitcher, G., Zhou, M. (Eds.), *Global ecology and oceanography of harmful algal blooms*. Ecol. Stud. 232, 229–259. https://doi.org/10.1007/978-3-319-70069-4_12

Gokul, E.A., Raitsos, D.E., Gittings, J.A., Hoteit, I., 2020. *Developing an atlas of harmful algal blooms in the red sea: Linkages to local aquaculture*. Remote Sens. 12 (22), 3695. https://doi.org/10.3390/rs12223695

Gomaa, M.N., Hannachi, I., Carmichael, W.W., Al-Hazmi, M.A., Abouwarda, A.M., Mostafa, E.A., Mohamed, H.E., Sheikho, K.M., Mulla, D.J., 2018. *Low diversity triggers harmful algae bloom (HAB) occurrence adjacent to desalination plants along the Red Sea*. Desalin. Water Treat. 114, 1–12. https://doi.org/10.5004/dwt.2018.22323

Häder, D.P., Gao, K., 2015. *Interactions of anthropogenic stress factors on marine phytoplankton*. Front. Environ. Sci. 3, 14. https://doi.org/10.3389/fenvs.2015.00014

Henson, S.A., Cael, B.B., Allen, S.R., Dutkiewicz, S., 2021. *Future phytoplankton diversity in a changing climate*. Nat. Commun. 12 (1), 5372. https://doi.org/10.1038/s41467-021-25699-w

Ismael, A.A., 2015. *Phytoplankton of the Red Sea*. [In:] Rasul, N., Stewart, I. (Eds.), *The Red Sea: the formation, morphology, oceanography and environment of a young ocean basin*, 567–583. https://doi.org/10.1007/978-3-662-45201-1_32

Ismael, A., Alkawri, A., 2024. *Harmful algae in the Red Sea*. [In:] Rasul, N., Stewart, I. (Eds.), *Coral reefs and associated marine fauna around the Arabian Peninsula*, CRC Press, 257–266. https://doi.org/10.1201/9781003321392

Kheireddine, M., Mayot, N., Ouhssain, M., Jones, B.H., 2021. *Regionalization of the Red Sea based on phytoplankton phenology: a satellite analysis*. J. Geophys. Res. Oceans, 126 (10), e2021JC017486. https://doi.org/10.1029/2021JC017486

Kheireddine, M., Ouhssain, M., Claustre, H., Uitz, J., Gentili, B., Jones, B.H., 2017. *Assessing pigment-based phytoplankton community distributions in the Red Sea*. Front. Mar. Sci. 4, 132. https://doi.org/10.3389/fmars.2017.00132

Khomayis, H.S., 2002. *The annual cycle of nutrient salts and chlorophyll a in the coastal waters of Jeddah, Red Sea*. JKAU: Mar. Sci. 13, 131–145.

Kürten, B., Khomayis, H.S., Devassy, R., Audritz, S., Sommer, U., Struck, U., El-Sherbiny, M.M., Al-Aidaroos, A.M., 2015. *Ecohydrographic constraints on biodiversity and distribution of phytoplankton and zooplankton in coral reefs of the Red Sea, Saudi Arabia*. Mar. Ecol. 36 (4), 1195–1214. https://doi.org/10.1111/maec.12224

LeGresley, M., McDermott, G., 2010. *Counting chamber methods for quantitative phytoplankton analysis – haemocytometer, Palmer-Maloney cell and Sedgewick-Rafter cell*. [In:] Karlson, B., Cusack, C., Bresnan, E. (Eds.), *Microscopic and molecular methods for quanti-*

tative phytoplankton analysis. IOC Manuals and Guides, 55, UNESCO, Paris, 25–30.

Mohamed, Z.A., 2018. *Potentially harmful microalgae and algal blooms in the Red Sea: Current knowledge and research needs*. Mar. Environ. Res. 140, 234–242. https://doi.org/10.1016/j.marenvres.2018.06.019

Morcos, S.A., 1970. *Physical and chemical oceanography of the Red Sea*. Oceanogr. Mar. Biol. Annu. Rev. 8 (73), 202.

Mudarris, M.S., Turki, A.J., 2006. *Sewage water quality and its dilution in the coastal waters of South Corniche, Jeddah, Red Sea*. JKAU: Mar. Sci. 17 (2), 11–128.

Naselli-Flores, L., Padisák, J., 2023. *Ecosystem services provided by marine and freshwater phytoplankton*. Hydrobiologia 850 (12), 2691–2706. https://doi.org/10.1007/s10750-022-04795-y

Orif, M.I., Kavil, Y.N., Al-Farawati, R.K., Sudheesh, V., 2023. *Deoxygenation turns the coastal Red Sea lagoons into sources of nitrous oxide*. Mar. Pollut. Bull. 189, 114806. https://doi.org/10.1016/j.marpolbul.2023.114806

Parsons T.R., Maita, Y., Lalli, C.M., 1984. *A manual of chemical and biological methods for seawater analysis*. Pergamon, Oxford, 173 pp. https://doi.org/10.25607/OBP-1830

Peña-García, D. 2022. *Nutrient gradients in the Red Sea: The coastal area off Jeddah and the central Red Sea*. Ph.D. Dissert., Christian-Albrechts-Universität zu Kiel.

Peña-García, D., Ladwig, N., Turki, A.J., Mudarris, M.S., 2014. *Input and dispersion of nutrients from the Jeddah Metropolitan Area, Red Sea*. Mar. Pollut. Bull. 80 (1–2), 41–51. https://doi.org/10.1016/j.marpolbul.2014.01.052

Post, A.F., Dedej, Z., Gottlieb, R., Li, H., Thomas, D.N., El-Absawi, M., El-Naggar, M., El-Gharabawi, M., Sommer, U., 2002. *Spatial and temporal distribution of Trichodesmium spp. in the stratified Gulf of Aqaba*. Red Sea. Mar. Ecol. Prog. Ser. 239, 241–250. https://doi.org/10.3354/meps239241

Racault, M.F., Raitsos, D.E., Berumen, M.L., Brewin, R.J., Platt, T., Sathyendranath, S., Hoteit, I., 2015. *Phytoplankton phenology indices in coral reef ecosystems: Application to ocean-color observations in the Red Sea*. Remote Sens. Environ. 160, 222–234. https://doi.org/10.1016/j.rse.2015.01.019

Raitsos, D.E., Hoteit, I., Prihartato, P.K., Chronis, T., Triantafyllou, G., Abualnaja, Y., 2011. *Abrupt warming of the Red Sea*. Geophys. Res. Lett. 38 (14). https://doi.org/10.1029/2011GL047984

Rasul, N.M., Stewart, I.C., Vine, P., Nawab, Z.A., 2018. *Introduction to oceanographic and biological aspects of the Red Sea*. [In:] Rasul, N., Stewart, I. (Eds.) *Oceanographic and biological aspects of the Red Sea*. Springer, Cham, 1–9. https://doi.org/10.1007/978-3-319-99417-8_1

Reynolds, C.S., 2008. *A changing paradigm of pelagic food webs*. Int. Rev. Hydrobiol. 93 (4--5), 517–531. https://doi.org/10.1002/iroh.200711026

Richardson, T.L., 2019. *Mechanisms and pathways of small-phytoplankton export from the surface ocean*. Annu. Rev. Mar. Sci. 11 (1), 57–74. https://doi.org/10.1146/annurev-marine-121916-063627

Richardson, T.L., Jackson, G.A., 2007. *Small phytoplankton and carbon export from the surface ocean*. Science 315 (5813), 838–840. https://doi.org/10.1126/science.1133471

Robinson, C., 2017. *Phytoplankton biogeochemical cycles*. [In:] Castellani, C., Edwards, M. (Eds.), *Marine plankton: A practical guide to ecology, methodology, and taxonomy*. Oxford Univ. Press, 42–51.

Salmaso, N., Tolotti, M., 2021. *Phytoplankton and anthropogenic changes in pelagic environments*. Hydrobiologia 848 (1), 251–284. https://doi.org/10.1007/s10750-020-04323-w

Schoo, K.L., Malzahn, A.M., Krause, E., Boersma, M., 2013. *Increased carbon dioxide availability alters phytoplankton stoichiometry and affects carbon cycling and growth of a marine planktonic herbivore*. Mar. Biol. 160, 2145–2155. https://doi.org/10.1007/s00227-012-2121-4

Smayda, T.J., 2008. *Complexity in the eutrophication–harmful algal bloom relationship, with comment on the importance of grazing*. Harmful Algae 8 (1), 140–151. https://doi.org/10.1016/j.hal.2008.08.018

Sofianos, S.S., Johns, W.E., 2003. *An oceanic general circulation model (OGCM) investigation of the Red Sea circulation: 2. Three-dimensional circulation in the Red Sea*. J. Geophys. Res. Oceans, 108 (C3).

Sofianos, S.S., Johns, W.E., Murray, S.P., 2002. *Heat and freshwater budgets in the Red Sea from direct observations at Bab el Mandeb*. Deep-Sea Res. Pt. 2, 49 (7–8), 1323–1340. https://doi.org/10.1016/S0967-0645(01)00164-3

Taylor, F.J.R., 1976. *Dinoflagellates from the international Indian Ocean expedition. A report on material collected by the R.V. "Anton Bruun" 1963–1964*. Bibl. Bot. 132, 1–234.

Tomas, C.R., 1997. *Identifying marine phytoplankton*. Acad. Press, New York, 858 pp.

Turki, A.J., Mudarris, M.S.A., 2008. *Bacteria and nutrients as pollution indicators in the Al-Nawrus recreational lagoon, Jeddah*. JKAU: Mar. Sci. 19 (1), 77–93.

Wafar, M., Ashraf, M., Manikandan, K.P., Qurban, M.A., Kattan, Y., 2016. *Propagation of Gulf of Aden Intermediate Water (GAIW) in the Red Sea during autumn and its importance to biological production*. J. Mar. Syst. 154, 243–251. https://doi.org/10.1016/j.jmarsys.2015.10.016